Preprint
UCRL-JC-135029

Electron, Photon, and Ion Beams from the Relativistic Interaction of Petawatt Laser Pulses with Solid Targets

S.P. Hatchett, C.G. Brown, T.E. Cowan, E.A. Henry, J. Johnson, M.H. Key, J.A. Koch, A.B. Langdon, B.F. Lasinski, R.W. Lee, A.J. Mackinnon, D.M. Pennington, M.D. Perry, T.W. Phillips, M. Roth, T.C. Sangster, M.S. Singh, R.A. Snavely, M.A. Stoyer, S.C. Wilks and K. Yasuike

U.S. Department of Energy

Lawrence
Livermore
National
Laboratory

This article was submitted to
American Physical Society 41st Annual Meeting of the Division of Plasma Physics
Seattle, WA
November 15-19, 1999

November 12, 1999

Electron, photon, and ion beams from the relativistic interaction of Petawatt laser pulses with solid targets*

Stephen P. Hatchett†, Curtis G. Brown,Thomas E. Cowan,Eugene A. Henry, Joy Johnson, Michael H. Key, Jeffrey A. Koch, A. Bruce Langdon, Barbara F. Lasinski, Richard W. Lee, Andrew J. Mackinnon, Deanna M. Pennington, Michael D. Perry, Thomas W. Phillips, Markus Roth‡, T. Craig Sangster, Mike S. Singh, Richard A. Snavely, Mark A. Stoyer, Scott C. Wilks, Kazuhito Yasuike‡

Lawrence Livermore National Laboratory , POBox. 808, Livermore Ca 94550, USA

In our Petawatt laser experiments several hundred joules of 1 μm laser light in 0.5–5.0 ps pulses with intensities up to $3x10^{20}Wcm^{-2}$ were incident on solid targets producing a strongly relativistic interaction. The energy content, spectra, and angular patterns of the photon, electron, and ion radiations were diagnosed in a number of ways, including several novel (to laser physics) nuclear activation techniques. From the beamed bremsstrahlung we infer that about 40-50% of the laser energy is converted to broadly beamed hot electrons. Their direction centroid varies from shot to shot, but the beam has a consistent width. Extraordinarily luminous ion beams almost precisely normal to the rear of various targets are seen — up to $3x10^{13}$ protons with kT_{ion} ~ several MeV representing ~6% of the laser energy. We observe ion energies up to at least 55 MeV. The ions appear to originate from the rear target surfaces. The edge of the ion beam is very sharp, and collimation increases with ion energy. At the highest energies, a narrow feature appears in the ion spectra, and the apparent size of the emitting spot is smaller than the full back surface area. Any ion emission from the front of the targets is much less than from the rear and is not sharply beamed. The hot electrons generate a Debye sheath with electrostatic fields of order MV per micron which apparently accelerate the ions.

---

* Paper FI2.04

† Invited speaker

‡ Permanent address: GSI Laboratory, Darmstadt, GERMANY

‡ Permanent address: 3-32-5 Uragamitai, Yokasuka, Kanagawa 239, JAPAN

I. INTRODUCTION

We have studied, in some detail, the x-ray emission from solid, "thick" (~1 mm) Au targets illuminated by the Petawatt laser. We report here on the characteristics of the bremsstrahlung and what it reveals about the hot electron flow within the target

In the process of attempting to observe relativistic (hereafter "hot") electron emission from solid, "thin" (~50–125 μm) Au and plastic (CH) targets we discovered extraordinarily luminous beams of ions from the backs of these targets. We discuss below the characteristics of the ion beams and our ideas on the mechanism generating them.

In our experiments with the Petawatt laser at Lawrence Livermore National Laboratory, several hundred joules of 1μm laser light in 0.5 and 5.0 ps pulses was focussed, at f/3, onto solid Au and CH targets. The laser focus had a broad spectrum of intensities reaching $3x10^{20}Wcm^{-2}$ in a central spot of 8 to 9 μm fwhm, with 25–30% of the pulse power inside the first minimum of the intensity pattern. Amplified spontaneous emission in a 4 ns period before the main pulse had about 10^{-4} of the main pulse energy, and there was a typically $3x\ 10^{-4}$ leakage pre-pulse 2 ns before the main pulse. (with factor of 3 shot-to-shot fluctuations). These generated a pre-formed plasma which was measured, by sub-picosecond pulse optical interferometry, to have an on axis electron density of $3\ x10^{19}\ cm^{-3}$ in a plane 70 μm from a flat CH target, with an approximately exponential fall to lower densities having a scale length of 40 μm.

Interaction of the main laser pulse with the preformed plasma and solid target generated a source of relativistic electrons directed mainly into the target which in turn generated bremsstrahlung x-rays in the target. Relativistic self focussing in the preformed plasma[1] will act to increase the intensity. This is evidenced in our work by an invariant x-ray emission spot of about 20 μm diameter (with suggestions of a substructure of multiple spots due to relativistic filaments) as the focal plane was displaced as much as 300 μm in front of the target[2]. Targets were typically "thick" or "thin"as above and 1 or more mm in the transverse directions.

We interpret our results in the context of particle-in-cell (PIC) calculations[3] that have indicated that at the relevant laser intensities the hot electron spectrum generated has a logarithmic slope temperature that is roughly equal to the ponderomotive potential in the laser beam. This is the cycle-averaged kinetic energy of an electron oscillating in the laser electromagnetic field:

$T_{hot} \approx U_{pond} \approx 1\mathrm{MeV} \times \left(I\lambda^2 / 10^{19} \mathrm{W\,c\,m^{-2}\,\mu m^2} \right)^{1/2}$ in the relativistic regime. The detailed spectral shape is not fully known. Earlier experiments which measured K-α lines excited by the hot electrons[4] were consistent with either a Boltzmann distribution, $N(E_e) \sim \exp(-E_e / kT_{hot})$, or a maxwellian distribution (relativistic) with the same average electron energy $\langle E_e \rangle$ (not the same temperature parameter).

II. ELECTRON AND PHOTON BEAMS — BREMSSTRAHLUNG ANALYSIS

Analysis of the bremsstrahlung emissions from high-Z targets has revealed much about the flow of relativistic electrons within them. We have used the experimental setup shown schematically in Fig. 1a, and several variations on that theme, to measure the spatial distribution of the bremsstrahlung together with some spectral information.

In this technique[5] the gold discs are activated by $Au^{197}(\gamma,xn)$ reactions. If a large number of discs is used, then usually only the (γ,n) reaction with a threshold of about 8 MeV has enough signal to be reliably counted. The response of the shielded TLD (thermo-luminescent dosimeter) array has been modelled with the Integrated Tiger Series[6] (ITS) of Monte-Carlo electron / photon transport codes, and we have found that the radiation exposure response has a sharp threshold at about 0.2 MeV and is essentially flat above 0.5 MeV. The shielding prevents a response to hot electrons from the target. This array then gives a measure of the integrated radiation above 0.2 MeV, while activation of the gold discs characterizes the bremsstrahlung in roughly the range of 10-16 MeV. Characteristic data from a particular shot are shown in Fig. 1b.

The ~10-16 MeV and broadband radiation are single peaked in the same, generally forward but somewhat off-axis direction. This behavior is typical. Further statistical analysis of the shot-to-shot variations in the direction of the peak and in its angular width show that in the ~10-16 MeV band the

direction centroid varies by ~±35º from the laser direction, but that the angular width is consistently about 100º fwhm. Since this bremsstrahlung is produced by highly relativistic electrons from which the radiation is strongly beamed in the electron velocity direction (to ±2º or less), this distribution must characterize the paths of those relativistic electrons within the target. This directional spread of relativistic electrons is very similar to that seen by Lasinski *et al* in 2-D PIC calculations of intensities in the range of 10^{21} Wcm^{-2} incident on overdense plasmas.[7] The pattern of broadband radiation seen by the TLD array has roughly the same central peak width but broader wings, which is expected because the wings must be produced by less relativistic electrons. In a few experiments there was sufficient signal from (γ,3n) activation corresponding to ~25–35 MeV, and the peaks from (γ,n) and (γ,3n) overlapped. Very occasionally, the radiation shows two well separated peaks. Almost all these sorts of experiments were conducted at normal incidence so we can say little about systematic behavior related to polarization or angle of incidence.

The ~±35º variation in beam direction appears to be evidence that the responsible relativistic electrons were not generated out in subcritical plasma but rather were promoted where the laser is beginning to penetrate relativistically overdense plasma. The phenomenon is again similar to that seen in PIC calculations reported by Lasinski *et al*[8] where the laser beam and hot electrons from overdense penetration are deflected by similar amounts. Both the data and the simulations suggest that under our conditions the deflection is a limited instability with random behavior.

In a variation on the above experimental setup there is a larger nickel disc in front of the array of gold discs which is also activated. The cross section for Ni^{58}(γ,n) peaks roughly in the range of 16-25 MeV. Therefore by comparing the average activation of the gold behind the nickel disc to the activation of the nickel and assuming a simple two parameter spectral form for the bremsstrahlung, say an overall constant and an exponential "temperature" $I_0 \exp(-h\nu / T)$, one can use the known cross-sections as a function of energy to fit a spectrum to the data. When this is done, the "temperature" characterizing the radiation in this ~10-25 MeV range is found to be ~4±1 MeV, roughly independent of incident laser energy, cf. Fig. 2. The ponderomotive scaling mentioned above would imply that the temperature only scales as the square root of the laser energy, but not even that is apparent given the scatter. The overall intensity I_0 shows order of magnitude shot-to-shot variation for the same laser energy, although the

upper envelope of the data appears to increase with laser energy. We note that choosing a value of $5x10^{11}$ for I_0 and 4 MeV for T gives 1.3 J/sr when integrated across the whole spectrum and >5J when integrated over all directions assuming a 100º FWHM.

Figure 3 shows the forward hemisphere average rads-at-1-meter seen by the TLD array plotted against laser energy for a number of shots. There is factor of two scatter at constant laser energy and no apparent corelation with laser energy in the 200-500 J range, but the overall average of about 0.45 rads at 1 meter suggests a rather high conversion efficiency of 40-50% from laser energy into hot electrons producing roughly 11 Joules of x-rays. This is consistent with the value derived from the activation data.

We estimate this conversion efficiency in the following way. From the measured laser spot size in vacuum, laser energy, and pulse length we derive a spectrum of laser intensities. Using the ponderomotive scaling above we generate a spectrum of hot electrons from a superposition of exponential (Boltzmann) electron spectra. We then use the ITS code to propagate this hot electron spectrum through the target generating bremsstrahlung and then fold the calculated bremsstrahlung output per Joule of hot electrons with the calculated TLD response and with the activation cross sections and compare to the data. Following this procedure naively we would calculate an impossible >100% conversion efficiency, and so we are forced to account for the known substantial self-focussing of the laser in the pre-plasma. On assuming that the laser is self-focussed in filaments to intensities 2-4 times nominal (conserving overall laser energy) we derive the 40-50% cited above. We note that the 4 MeV x-ray slope temperature observed, if equated to an electron slope temperature, corresponds to U_{pond} at an intensity of $1.6x10^{20}$, half the *peak* and much greater than the *mean* energy-weighted vacuum intensity.

The ITS modeling approach has a serious limitation: This code treats the electrons as independent and so it is not *a priori* self-consistent with the electro-magnetic fields generated by the production and transport of the hot electrons. Nevertheless, as long as the electrons have forward directed paths, as shown by the photon beaming in the data, the conversion effeciency estimate will not be far wrong.

In summary, the bremsstrahlung measurements show several characteristics of the hot electrons generated in the interaction with solid, high-Z targets. A large fraction of the laser energy is converted to hot electrons. The paths of the hot electrons are broadly beamed, not tight spirals or corkscrews in their self-generated magnetic field. The bulk of the hot electrons have mean energies a few times that given by

the ponderomotive scaling assuming vacuum laser intensities. Most of the electrons up to several times the self-focussed ponderomotive potential appear to be generated where the laser penetrates overdense plasma, and there is an instability there causing a deflection of the beam.

III. ION EMISSION — DATA

The proton beam was detected first by an experiment designed to measure the spectrum and angular pattern of hot *electrons* ejected from thin targets. The setup used a multilayer conical assembly of 100 μm thick Ta foils and absolutely calibrated radiochromic (RC) film as shown in Fig. 4 . The RC film changes from transparent to dark blue in proportion to the dose of absorbed energy from ionising radiation of any kind. The film data were analysed by digital densitometry. Results are discussed by Snavely *et al*[9]

A collimated intense beam, as seen in Fig. 4, was emitted perpendicular to the rear surface of the target for both normal and 45^0 incidence and laser energies from ~150 J to ~750 J on Au and CH targets of thickness ranging from 20 to 120 μm. The angular width narrows sharply in images recorded through greater thicknesses of Ta. Penetration generally increased with laser energy. From Au targets the beam is very uniform in intensity with smooth, sharp boundaries, but from CH targets it exhibits internal fine strucure and more ragged edges. (This is illustrated in Fig. 6. below.)

The proton identity of the beam was first suggested by analysis of etched tracks in CR39 plastic behind 7mm of Al which gave evidence of > 30 MeV protons.

We modelled the response of the RC film / tantalum packages with the SRIM[10] monte-carlo ion transport code, assuming the beam to be protons, and obtained response functions for the layers of RC film similar to those shown in Fig. 5(a). Fitting modelling to experimental data for the conditions of Fig 4. (Au target at 45^o incidence) gave a plausible proton beam energy content of 10J with an exponential slope temperature of about 4 MeV.

Direct evidence that the beam is comprised of protons was obtained from observation of proton induced nuclear reactions. In a variation on the setup of Fig. 4. we fielded a flat, multilayer detector consisting of 50 μm Ti, followed by 3 repeats of (1.5 mm Be, 250 μm Ti, 250 μm RC film),then a final 1.5 mm Be and 250μm RC film, This was placed placed 3 cm behind the target which was illuminated at

normal incidence. The yield of the nuclear process, Ti^{48} (p,n) V^{48} was measured absolutely from the characteristic gamma emission of the activated V^{48} nuclei. The cross section has a threshold at 5 MeV and has a peak of ~500 mb at 12 MeV, and with the known cross section we calculated the activation response of each Ti layer with the SRIM code similarly to our calculation of the RC film response. Results are shown in Fig 5(b). The measured numbers of activated nuclei in the Ti layers were compared to the modelling to find a simple exponential spectrum fit. The largest yields were obtained for normal incidence on 55 μm thick CH targets. The maximum penetration of the beam showed that there were proton energies >40MeV, and the attenuation with thickness indicated a slope temperature of ~6 MeV. The absolute number of activated nuclei showed that there was a total of $3x10^{13}$ protons (or 30J of energy) which was 7% of the laser energy incident on the target. A further nuclear based diagnostic was the observation of $3x10^{10}$ neutrons in a Ag activation neutron detector. This yield was attributed to several neutron producing channels of proton interaction with Be nuclei and was an order of magnitude greater than the neutron yield without Be present. Clear confirmation that the beam angular pattern seen in the RC film images is due to protons was obtained from autoradiography images of the activation in the Ti foils as seen in Fig. 6 which shows the exact correspondence of RC film images and autoradiographs from adjacent layers of the detector on a single shot .

Specific attention was directed to whether the beam was normal to the front or the rear surface of the target using the 2 mm wide 30^{o}wedge target of CH shown schematically in Fig. 7. Clear evidence that the emission was normal to the rear surface is seen in the two separate proton beams in directions corresponding to the normals to the major and minor “rear” surfaces of the wedge.

The spatial origin of the protons was evidenced further in RC images from 1 mm square thin foil targets via the thinnest filters used (25 μm Al recording protons with energy > 4MeV) . In addition to the intense beam, a weaker *sheet* of proton emission was seen in the horizontal plane which we attribute to the vertical edges of the target. These data show that there is proton emission from an extended area of the rear surface of the target but that lower energy protons are emitted further from the center.

We looked for ion emission off the front of the target, in the direction back toward the laser beam. There was no proton beam detectable above the backgound exposure level due to hot electrons. A test using cones of RC film placed both behind and (with a central hole for the laser beam) in front of a CH target irradiated at 45^{0} established that protons above the 4 MeV threshold energy for detection,

integrated over the forward hemisphere, had less than 5% of the energy recorded in the proton beam from the rear surface.

A magnetic spectrometer, mounted on the side of the target chamber at 45º to downstream laser axis (and originally fielded to measure the electron and positron emission from the targets) was adapted to detect protons, and it has been a rich source of energetic proton data. Unambiguous confirmation of protons from the target was obtained by recording the energy spectrum of the protons reaching the spectrometer via a hole in the RC film detector of Fig. 4. Conventional film over nuclear emulsion was placed in the proton detection plane, and data were obtained from analysis of tracks in the emulsion and exposure of the film. For targets irradiated at 45º incidence the instrument recorded the energy spectrum on the axis of the proton beam while for targets at normal incidence it recorded the spectrum 45º off axis . A sharp cut off at high energy was observed in all cases. There was also evidence of a narrow peak in the spectrum at the maximum energy. Unfortunately, only a few MeV below the high energy cutoffs the films and nuclear emulsions were saturated, and we can say little about the overall spectra. The maximum energy recorded on the beam axis was 55 MeV falling to 15 MeV at 45^0.

Near the high energy cutoff, where saturation is not an issue, and in the direction perpendicular to the magnetic dispersion, the edges of the spectrometer slit form a penumbral image of the proton emitting region. We have analyzed a shot in which the target was a 4mm x 4mm x 125μm thick slab of Au illuminated at 45º (so the spectrometer was looking at the beam). Near the 20 MeV cutoff, the size of the emitting spot was less than 400 μm diameter, and perhaps less than 300 μm, — much smaller than the whole back surface of the target.

IV. ION EMISSION — MECHANISM AND DISCUSSION

We interpret the process generating the proton beam as a new variation on a familiar theme — acceleration by a sheath electrostatic field generated by the hot electrons. The interaction of the focused main pulse with the pre-formed plasma and the underlying solid generates an intense hot electron source with an energy spectrum related to the laser intensity as described above. At a conversion efficiency of around 40% and with an exponential slope temperature of a few MeV (consistent with the bremsstrahlung results discussed above) a few x 10^{14} hot electrons will be generated. Only a very small fraction of these can leave the target before the resulting Coulomb potential traps the rest. They will fly through the thin targets in a broad angular beam like that seen in the bremsstrahlung data, be turned

around near the back, and bounce back and forth through the target drifting transversely. Given the volume of our thin targets, they will have a density of several x 10^{18} cm^{-3}. We expect that as the hot electrons tend to relax to Boltzmann equilibrium, $N_{e,hot} \sim \exp\left(-e\Phi/kT_{hot}\right)$, they will set up a sheath at the target surface with a scale length given by the Debye length of the hot electrons:

$$\ell_0 \equiv \left(\frac{kT_{hot}}{4\pi e^2 N_{e,hot}}\right)^{1/2} = 2.4\mu m \left(\frac{kT_{hot}}{1\,MeV}\right)^{1/2} \left(\frac{N_{e,hot}}{10^{19}\,cm^{-3}}\right)^{-1/2} \qquad \frac{U_{pond}}{\sqrt{E_{laser}}} \sim const.$$

The combination of high hot electron density and relativistic temperature will establish a very strong sheath electrostatic field:

$$\mathbf{E} \approx \frac{kT_{hot}}{e\ell_0} = \frac{\text{Megavolts}}{\text{microns}}; \quad \mathbf{E} \quad E_{laser}^{1/2}$$

This field is very much larger than the field created by the initially escaping electrons for which the scale length in the denominator is the target size.

We attribute the fast ion acceleration to this field. What is new is that the hot electrons are effectively created in a delta-function time pulse and they have ranges much greater than the target thickness.

We believe that the ponderomotive force process at the front surface of the target is *not* producing the observed ions for several reasons. First, there is clear evidence that the protons are emitted perpendicular to the *rear* surface(s) of the target. Second, evidence of proton emission from the edges of the target supports a model of emission over an extended area much larger than the focal spot (at least for the lower energy ions). Finally, protons are detected from *gold* targets, which is understood to be emission from a layer of adsorbed molecules containing hydrogen. This could not come from the front surface focal region of our targets because the pre-pulse would blow off such monolayers into pre-formed plasma. Moreover, an area which is much larger than the 10^{-6} cm^2 focal spot area would be needed to supply the observed number of protons from an adsorbed impurity layer.

A full discussion of this model is in preparation by the authors; we outline a quasi-1-D version below. We suppose that on all target surfaces there is an initial density gradient — very steep on the back of the target, less steep on the front. Figure 8 illustrates the solution derived from Poisson's equation and Boltzman statistics for the electrons. A suddenly created hot electron density floods through the target and, in a pre-existing density gradient, excludes the cold electrons at ion densities lower than the hot

electron density. Further out, the hot electron density will fall with the ion density (quasineutrality) until the *local* hot electron Debye length becomes greater than the local ion scale length. There, a hot electron Debye sheath will form. The charge in this sheath will be balanced and retained by a positive charge sheet which forms where the cold electrons have become excluded. Between the sheath and positive ion charge sheet will be a region of ~constant E field with the magnitude of the field given by:

$$\mathbf{E} \approx kT_{hot}/e\ell_{Debye,local} \approx kT_{hot}/e\ell_{ion}$$

Ions in this region and ions from the charge sheet will be accelerated. Because the E field scales inversely with the density scale length ℓ_{ion}, there will be much stronger acceleration at the steep density interface on the *back* of the target, and it will result in a rate of energy transfer to ions which is initially much greater than at the front surface. If the hot electrons dissipate their energy rapidly, the result will be a larger energy transfer to ions at the back surface. This model also predicts that the ions located between the Debye sheath and the internal charge sheet will initially all have the same acceleration and so will create the observed narrow peak in the ion spectrum at the high energy cutoff. The steep ion front where the sheath separates is a familiar dynamical attractor as the acceleration proceeds, cf. Denavit[11] and references therein. It is observed as a high energy cutoff in the spectrum.

Ion acceleration will continue until the hot electrons are energetically depleted, by ranging out, by adiabatic cooling, or by accelerating ions. Simple estimates indicate that for our conditions the last process dominates, and the time scale is a few ps. Given the field strength estimated above for a few micron (or less) density scale length (back of the target), this corresponds to accelerating protons to several tens of MeV, with the proton energy scaling like the square of the field strength. On the other hand, on the front of the target, with density scale lengths of several tens of microns, the peak ion energy will be sub-MeV.

This quasi-1-D picture thus accounts semi-quantitatively for many of the observed features of the ion beams — the front-back asymmetry, the narrow feature in the energy spectrum at the high energy end, and the high energy cutoff.

Of course, this model does not account for some important 2(3)-D features of the data. The emitting spot is apparently much smaller than the target at the highest ion energies, but the lowest energy ions are emitted all the way out at the target edges. Furthermore, the size of the ion beam decreases with increasing energy. This is clear from the data illustrated in Fig. 4 and the response functions shown in

Fig.5: For a falling ion spectrum each layer is primarily responding to the narrow part of the ion spectrum under the cusp in the response function. Pending further investigation, we speculate that the former effect is simply due to the fact that ion acceleration off the back begins as soon as hot electrons reach it, and that, given the electron beaming behavior described above, this happens first in a region of diameter of roughly 2 x target-thickness x tan(50º)~300 μm. (We note here that a somewhat smaller region, 100 μm diameter at 100 μm depth, of localized *heating* has been observed in buried layer experiments with the PW laser.[12]) The ions accelerated for the most time reach the highest energies. The second effect is apparently *not* due to a constant transverse momentum dispersion: The transverse momentum corresponding to the RC film spot edge decreases with increasing ion energy. More likely, the effect is due to coulomb forces within the beam, but this must await quantitative confirmation from multi-dimensional PIC calculations.

V. CONCLUSIONS

In our experiments laser energy incident on solid targets is efficiently converted to relativistic electron energy, apparently in the region of laser penetration into overdense plasma. The hot electrons created there are broadly beamed in a pattern consistent from shot-to-shot, but the beam direction is apparently randomly variable, within limits. The spectrum of similarly beamed electrons includes energies from well below the mean up to several times the mean energy indicating a common origin across that range. The electron energies are consistent with the ponderomotive potential scaling if relativistic self-focussing increases the nominal intensity by a factor of 2 or more.

The hot electrons are generated in sufficient numbers and energy to produce sheath electrostatic fields of order megavolts / micron, on surfaces where the density scale length is less than the Debye length of the hot electrons. These fields efficiently accelerate beams of ions from the surfaces up to many times the hot electron energies. The acceleration mechanism appears to be sufficiently simple, controllable, and efficient as to make it useful for applications in a variety of contexts[13]. More work is needed to characterise the beam emittance which will determine its focusability and its usefulness.

*Work performed for the U.S. D.O.E. by LLNL under Contract No. W-7405-ENG-48

FIGURE 1.

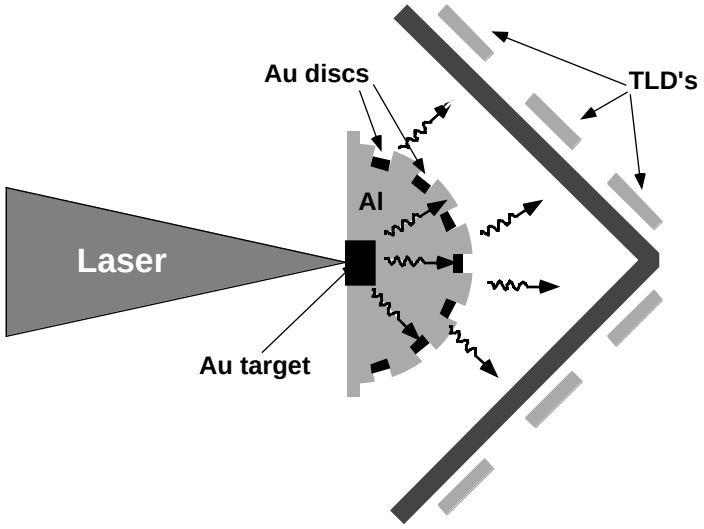
Au discs
TLD's
Al
Laser
Au target

.

,

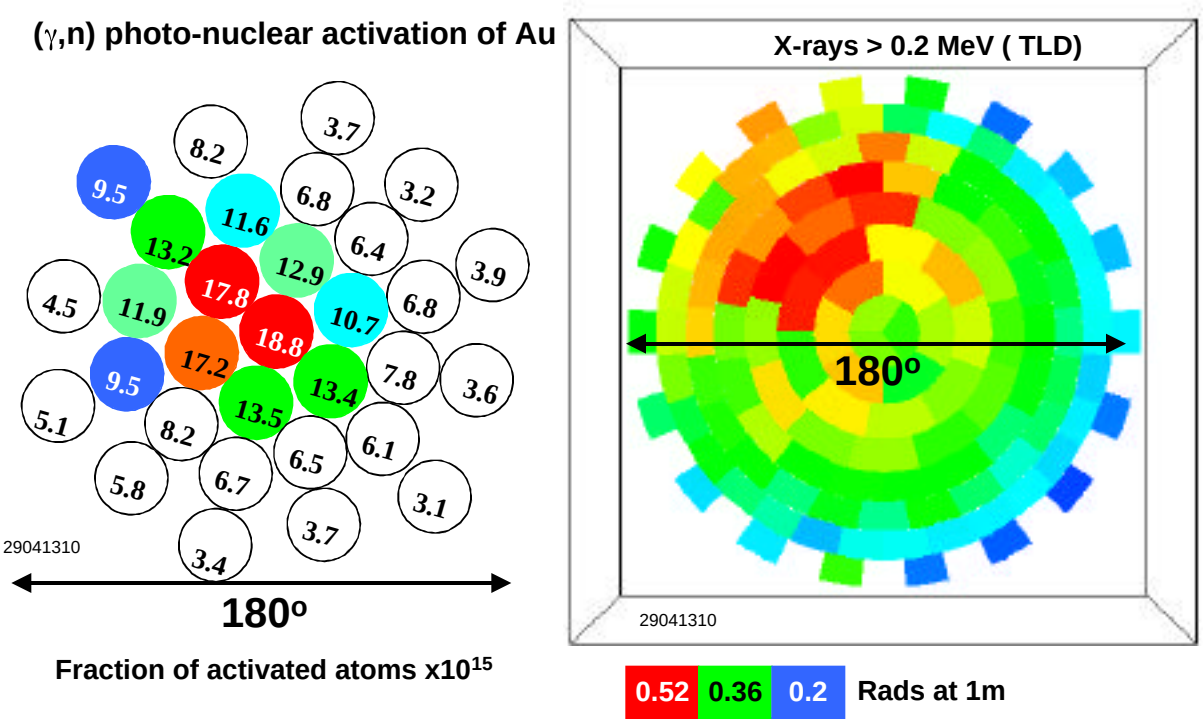
(γ,n) photo-nuclear activation of Au
9.5
8.2
3.7
11.6
6.8
3.2
13.2
6.4
12.9
3.9
4.5
11.9
17.8
10.7
6.8
18.8
17.2
9.5
7.8
3.6
13.4
5.1
13.5
8.2
6.1
6.5
5.8
6.7
3.1
3.7
3.4
29041310
180o
Fraction of activated atoms x10^15
X-rays > 0.2 MeV (TLD)
180o
29041310
0.52
0.36
0.2
Rads at 1m

FIGURE 2.

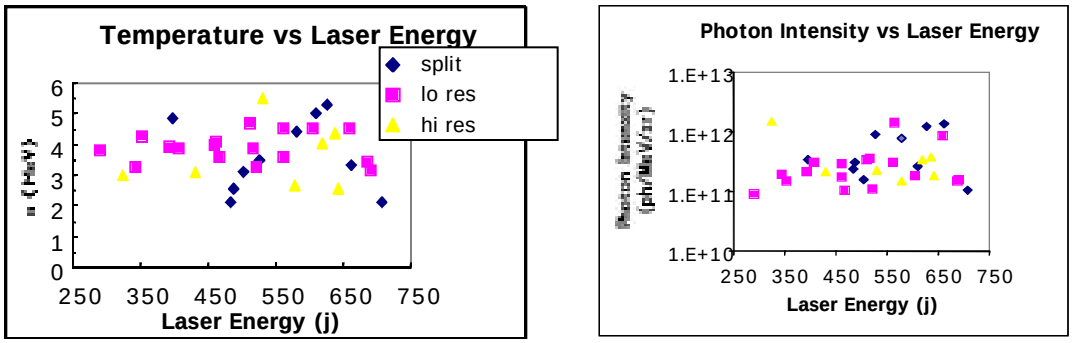

FIGURE 3.

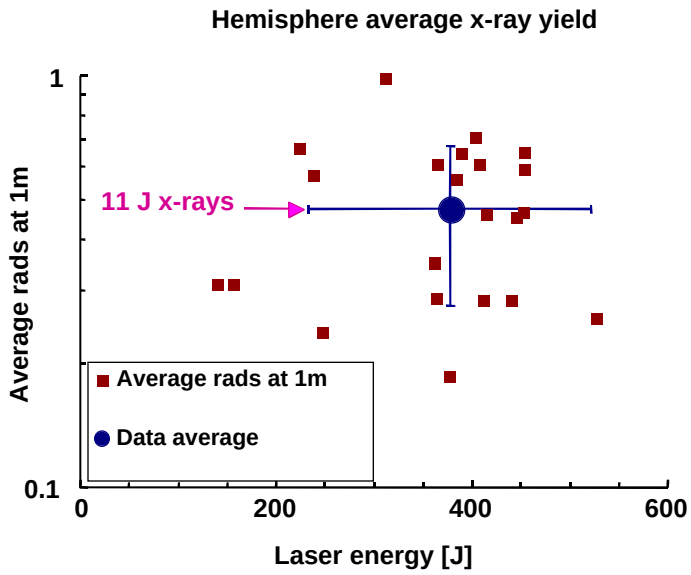

FIGURE 4.

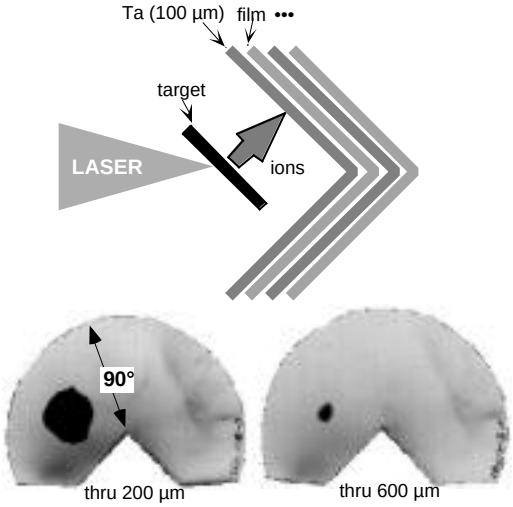

FIGURE 5.

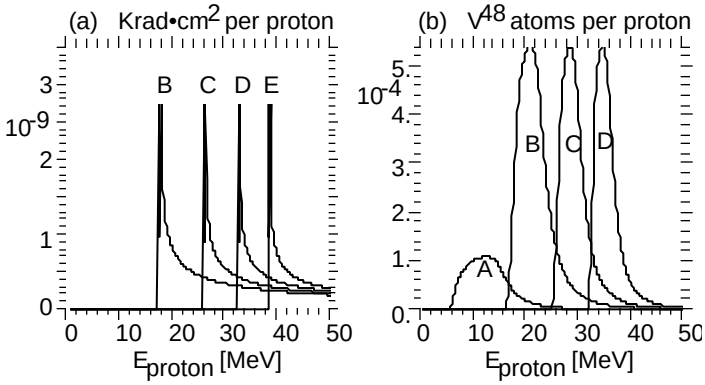

FIGURE 6.

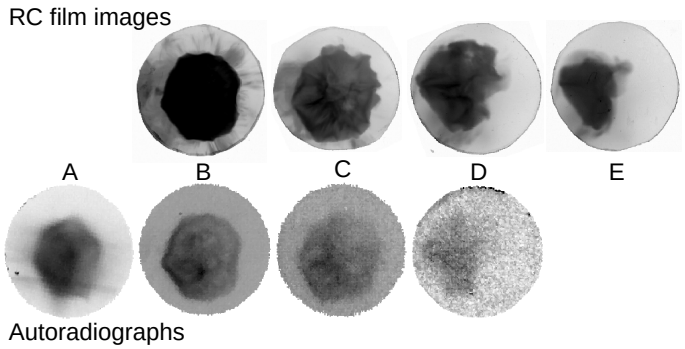

FIGURE 7.

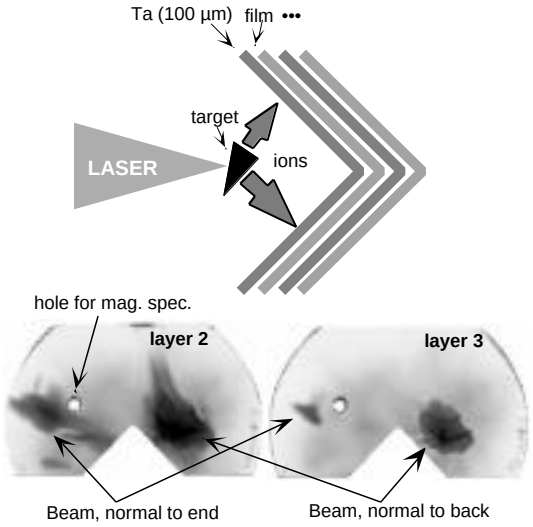

.

FIGURE 8.

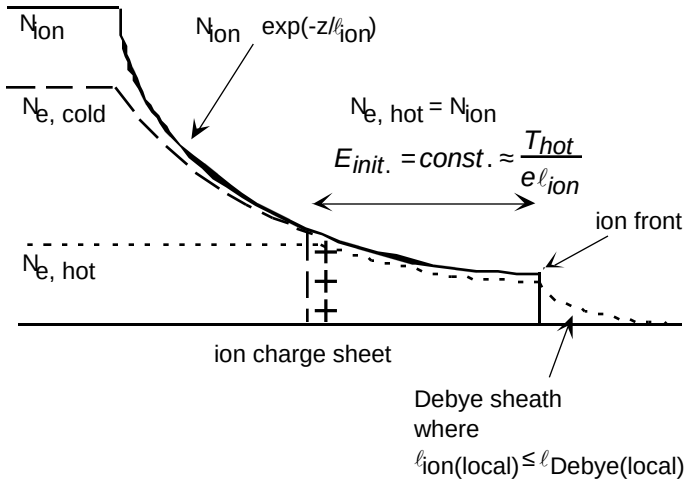
N ion
N ion exp(-z/ℓ ion)
N e, cold
N e, hot = N ion
E init. = const. ≈ T hot / e ℓ ion
ion front
N e, hot
ion charge sheet
Debye sheath
where
ℓ ion(local) ≤ ℓ Debye(local)

FIGURE CAPTIONS

Figure 1. (a) Schematic of experimental setup to measure the bremsstrahlung output from Au targets. The Au discs are activated and the shielded TLDs measure the integrated energy deposition by photons. (b) Typical results from a single shot showing the beam of activating x-rays (~10-16 MeV) and corresponding to the beam integrated over all energies >0.2 MeV.

Figure 2. Angle averaged slope temperature and intensity of bremsstrahlung in the 10-25 MeV range measured by activation of Au and Ni. The different symbols correspond to different sizes and arrangements of Au discs, but in all cases the average includes the intensity peak and surrounding solid angle.

Figure 3. Average rads-at-1-meter seen by the TLD array plotted against incident laser energy and showing the average and standard deviation for the shots on which these quantities were measured. From ITS modelling we derive an estimate of 11 Joules of x-rays and hence a 40-50% conversion efficiency, as described in the text.

Figure 4. Schematic of the RC film detection system and RC film "images" through 200 μm Ta (>14MeV) and 600 μm Ta (>26 MeV). Arrow indicates 90^{o} angle range seen from target. Target was 1 mm square 125 mm thick Au foil irradiated at 45^{o} P polarized incidence.

Figure 5 Modelled response of RC film (a) and nuclear activation of Ti (b), under proton beam irradiation via attenuators used in the experiments . Layers A…E correspond to RC film images and autoradiographs shown in Fig. 6.

Figure 6 . Radiochromic film images (above) and corresponding autoradiographs of adjacent Ti foils (below) for a 55 μm CH target at normal incidence.

Figure 7. Wedge target schematic and RC film images via 200 and 300 μm Ta (protons >14 and >17 MeV).The image shows two proton beams , the larger from the major face and the smaller from the minor face of the wedge as indicated by the arrows

Figure 8. Schematic of the proton acceleratiuon model described in the text.

REFERENCES

[1] A Pukhov, J Meyer ter Vehn,Phys. Rev. Lett. 76,3975(1996)

[2] M H Key et al. Proc 17th IAEA Fusion Energy Conf. (In press).

[3] S.C. Wilks, W.L. Kruer, M. Tabak, and A.B. Langdon, Phys. Rev. Lett. **69**, 1383 (1992); S.C. Wilks, Phys. Fluids B **5**, 2603 (1993); S.C. Wilks and W.L. Kruer, IEEE J. Quantum Electron. **11**, 1954 (1997); B. F. Lasinski, A.B. Langdon, S.P. Hatchett, M.H. Key, and M. Tabak, Phys. Plasmas **6**, 2041, (1999).

[4] K.B. Wharton, S.P. Hatchett, S.C. Wilks *et al*, Phys. Rev. Lett. **81**, 822.(1998)

[5] T.W. Phillips, M.D. Cable, T.E. Cowan, S.P. Hatchett, E.A. Henry, M.H. Key, M.D. Perry, T.C. Sangster, and M.A. Stoyer, Rev. Sci. Instrum. **70**, 1213 (1999); M.A. Stoyer, T.C. Sangster, E.A. Henry *et al*, "Photonuclear Activation in Ultra-Intense Laser Experiments," submitted to Phys. Plasmas.

[6] J.A. Halbleib and T.A. Mehlhorn, Nucl. Sci. Eng. **92**, 338 (1986)

[7] B. F. Lasinski, A.B. Langdon, S.P. Hatchett, M.H. Key, and M. Tabak, Phys. Plasmas **6**, 2041, (1999)

[8] ibid

[9] R. A. Snavely, S. P. Hatchett, M. H. Key *et al*, Bull. Am. Phys. Soc. DPP Seattle meeting, paper Q01.12, (1999)

[10] J. F. Ziegler, J. P. Biersack and U. Littmark, *The Stopping and Range of Ions in Solids*, (Pergamon Press New York, 1996)

[11] J. Denavit, Phys. Fluids **22**, 1384 (1979)

[12] J.A. Koch, S.P. Hatchett, M.H. Key, R.W. Lee, D. Pennington, R.B. Stephens, and M. Tabak, "Observation of deep directional heating at near-solid density caused by laser-generated relativistic electrons", submitted to Phys. Rev. Lett.; .J.A. Koch, S.P. Hatchett, M.H. Key, R.W. Lee, D. Pennington, R.B. Stephens, and M. Tabak, Bull. Am. Phys. Soc. DPP Seattle meeting, paper UP2.36 (1999)

[13] T.E. Cowan, M. Roth, J. Johnson, "Laser acceleration of low emittance, monoenergetic proton beams", submitted to Nature.